Available online at www.sciencedirect.com
SCIENCE DIRECT®
International Journal of Heat and Mass Transfer 49 (2006) 4407–4416
International Journal of HEAT and MASS TRANSFER
www.elsevier.com/locate/ijhmt

Study of close contact melting of ice from a sliding heated flat plate

Dominic Groulx, Marcel Lacroix *

Département de génie mécanique, Université de Sherbrooke, Sherbrooke, Québec, Canada J1K 2R1

Received 16 August 2005; received in revised form 8 May 2006
Available online 30 June 2006

Abstract

A study is conducted to examine the effect of the relative motion between a PCM block and a heated flat plate in the process of close contact melting of a high Prandtl number phase change material. An analytical model is proposed and experimental results are reported. Results indicate that the relative velocity between the PCM block and the plate starts to play an important role in the close contact melting process when $Re > 10^4$. Three distinct melting regimes are identified: for $Re < 3 \times 10^5$, close contact melting is the dominant mode of heat transfer in the melt layer. The relative motion may reduce the melting time by up to 66% compare to the melting time observed from a heated surface at rest. For $Re > 5 \times 10^5$, the thickness of the liquid melt layer is so small ($\delta^* < 8 \times 10^{-4}$) that the melting process is hindered and abrasion is observed. Finally, for $3 \times 10^5 < Re < 5 \times 10^5$, a transition regime bridges the contact melting regime to the abrasion regime.

Keywords: Contact melting; Sliding surface; Convection; Experiments

1. Introduction

For nearly three decades, solid–liquid phase change heat transfer has received increasing research attention in the open literature [1]. This type of heat transfer finds applications in the fusion of ice and the solidification of water [2–4], purification of metals [5], study of geophysical phenomena (fusion of glaciers and volcanic eruptions) [6], cooling of electronic equipments [7] and thermal control of space stations and vehicles [8–12]. One of the modes of heat transfer found in a system that undergoes solid–liquid phase change is close contact melting. Close contact melting occurs when a solid melts while being in contact with a heat source. The liquid generated at the melting front is squeezed out from under the solid by the pressure maintained in the central section of the film by the weight of the free solid. If the heat source moves relative to the melting solid, the liquid generated at the melting front is also dragged out from under the solid by the action of the moving heat source.

The problem of close contact melting has been the subject of a number of investigations related to the fundamentals of heat transfer [6,13–19,28–30], lubrication [1] and latent heat energy storage [20–22]. Close contact melting is primarily studied because the heat transferred across the melt layer separating the heat surface from the solid phase change material (PCM) is much higher than the heat transferred by convection, which generally occurs in much thicker layers of molten material. As a consequence of the higher heat fluxes, the melting time is considerably reduced.

In most of the previous studies on close contact melting, the process by which the melt is squeezed out of the small gap separating the heat source and the solid was assumed to be quasi-steady and the heat transfer through the liquid film was considered to be conduction dominated [1,6,14–23]. Recent studies suggest however that this last assumption may no longer be valid when a relative motion between the solid PCM and the heat source is imposed [24,25].

* Corresponding author. Tel.: +1 819 821 8000; fax: +1 819 821 7163.
E-mail address: Marcel.lacroix@usherbrooke.ca (M. Lacroix).

0017-9310/$ - see front matter © 2006 Elsevier Ltd. All rights reserved.
doi:10.1016/j.ijheatmasstransfer.2006.05.007

Nomenclature

Dimensional variables

C	heat capacity (J/kg K)
g	acceleration of gravity (m/s^2)
h	latent heat of fusion (J/kg)
H	initial height of the block (m)
k	thermal conductivity (W/m K)
L	length of the block (m)
n	constant determine experimentally
P	pressure (Pa)
Q	flow rates (m^2/s)
S	molten height of the block (m)
t	time (s)
T	temperature (K)
u	x velocity component (m/s)
v	y velocity component (m/s)
U	speed of the liquid in the gap (m/s)
V	melting speed (m/s)
$\widetilde{V}$	quasi-steady liquid velocity (m/s)
x	coordinate (m)
y	coordinate (m)

Greek symbols

α	thermal diffusivity of melt (m^2/s)
δ	molten layer thickness (m)
ΔT	temperature difference ($T_p - T_m$) (K)
Λ	effective height of the dragging effect (m)
μ	dynamic viscosity (N s/m^2)
ν	kinematic viscosity (m^2/s)
ρ	density (kg/m^3)

Non-dimensional variables

B	variable, argument of function F
$f_1(Ste,Re)$	function dependent on the Stefan and Reynolds number
$f_2(Ste)$	function dependent on the Stefan number
$F(B)$	function dependent on B

Subscripts

eff	effective
f	liquid
fs	liquid solid
m	melting point
p	plate
s	solid
sc	subcooled
x	in the x direction
z	in the z direction

Superscript

*	indicates dimensionless quantity

Definitions of non-dimensional variables

Nu	Nusselt number $q''/(k_f\Delta T/L_x)$
Pr	Prandtl number (ν/α)
Re	Reynolds number (UL_x/ν)
Ste	Stefan number ($C\Delta T/h_{fs}$)

Although, few studies have examined the effect of the relative motion between the PCM and the heated source on close contact melting [26,27], these investigations focused on the transient thermal behaviour in the early stages of close contact melting. Conduction was still considered to be the prevailing mechanism of heat transfer across the melt layer. Convection was ignored.

The two main objectives of the present study are, first, to report experimental results of close contact melting of ice heated from a moving heated flat plate and, second, to propose a mathematical model that predicts adequately the melting process. The melting of a high Prandtl number substance in contact with a moving heated surface is then studied and the effect of the relative motion is delineated in terms of the Stefan and Reynolds numbers.

2. Mathematical model

A schematic representation of the physical system is depicted in Fig. 1. A block of solid PCM of height H, length L_x and depth L_z is initially at a uniform subcooled temperature $T_m - T_{sc}$ and rests on a flat plate. At time $t = 0$, the temperature of the flat plate is suddenly raised to a constant value $T_p = T_m + \Delta T$ and simultaneously a relative motion between the plate and the PCM is set. The amplitude of the relative motion is U. Melting is triggered and the solid descends vertically at a speed V while squeezing the melt out of the thin gap of thickness δ between the solid and the plate.

Six assumptions are made regarding the behaviour of the physical system:

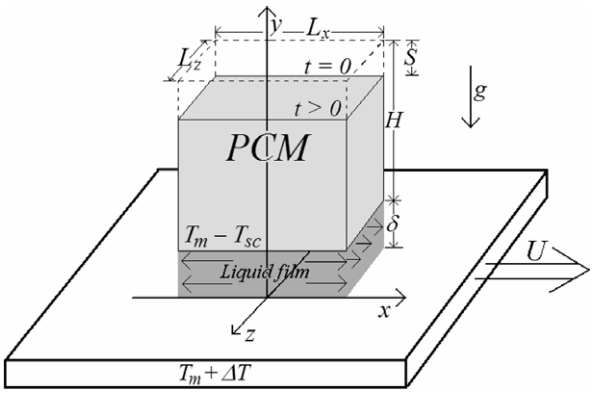

Fig. 1. Schematic of the system.

(1) The melting process is considered quasi-steady, i.e., at every point in time the weight of the solid is balanced by the excess pressure built in the liquid film.
(2) The heat transfer is one-dimensional (function of y only).
(3) Momentum and pressure variation are dominant in the direction of the motion of the flat plate, i.e. x-direction.
(4) The liquid film thickness δ is constant along the length L_x and L_z of the block (this assumption results from 2). δ may, however, vary with time.
(5) The flow in the liquid film remains laminar.
(6) The fluid properties are temperature independent and are evaluated at the film temperature ($T_{\text{film}} = T_{\text{m}} + \Delta T/2$).
(7) The temperature of the PCM block is considered constant throughout the melting process.

2.1. Conservation of energy

Subjected to the above assumptions, the energy conservation equation for the melt becomes [18]

$$v\frac{\partial T}{\partial y} = \alpha_{\text{f}}\frac{\partial^2 T}{\partial y^2} \tag{1}$$

for which the boundary conditions are $T(y=0) = T_{\text{p}} = T_{\text{m}} + \Delta T$ and $T(y=\delta) = T_{\text{m}}$. Furthermore, the velocity component v in Eq. (1) is approximated by the melting speed V at the melting interface ($y = \delta$).

The temperature distribution in the liquid gap is obtained from the solution of Eq. (1):

$$T(y) = T_{\text{m}} + \Delta T\frac{\{\exp(-Vy/\alpha_{\text{f}}) - \exp(-V\delta/\alpha_{\text{f}})\}}{1 - \exp(-V\delta/\alpha_{\text{f}})} \tag{2}$$

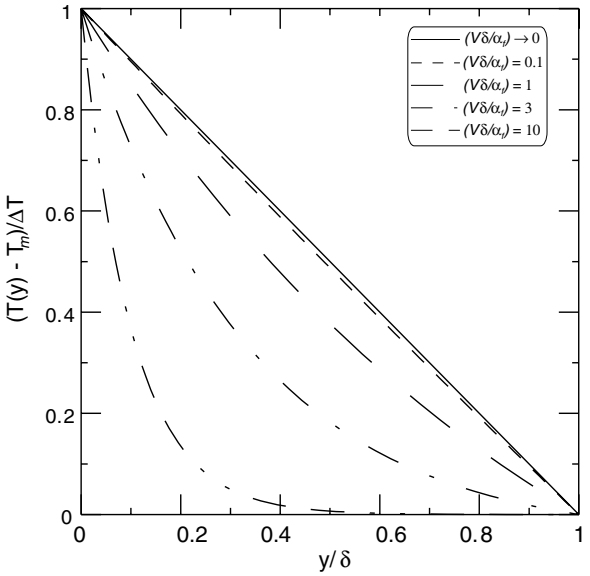

Fig. 2. Temperature profile in the melt layer.

This temperature profile is plotted in Fig. 2. It is seen that the effect of convection becomes increasingly important for $(V\delta/\alpha_{\text{f}}) > 0.1$. For these cases, the linear temperature profile assumed in previous models is no longer valid. Indeed, as the dimensionless parameter $V\delta/\alpha_{\text{f}}$ increases in magnitude, the mean temperature of the liquid in the melt gap gets closer to the melting point T_{m} and, as a result, the heat flux at the melting front diminishes and so the melting rate.

In addition, at the solid–liquid interface ($y = \delta$), an energy balance yields

$$-k_{\text{f}}\left(\frac{\mathrm{d}T}{\mathrm{d}y}\right)_{y=\delta} = \rho_{\text{s}}V(h_{\text{fs}} + C_{\text{s}}T_{\text{sc}}) \tag{3}$$

Substitution of Eq. (2) into Eq. (3) provides a first relation between the molten layer thickness δ and the melting speed V

$$-\rho_{\text{f}}C_{\text{f}}\frac{\Delta T}{1 - \exp(V\delta/\alpha_{\text{f}})} = \rho_{\text{s}}(h_{\text{fs}} + C_{\text{s}}T_{\text{sc}}) \tag{4}$$

2.2. Conservation of momentum

At all times, it is assumed that the pressure in the liquid gap is related to the weight of the PCM block by

$$L_z\int_{-\frac{L_x}{2}}^{\frac{L_x}{2}} P(x)\,\mathrm{d}x = \rho_{\text{s}}(H - S)L_xL_zg \tag{5}$$

Once again, subjected to the above assumptions, the momentum conservation equation for the melt may be expressed as [18]

$$\frac{\partial^2 u}{\partial y^2} = \frac{1}{\mu_{\text{f}}}\frac{\mathrm{d}P}{\mathrm{d}x} \tag{6}$$

The boundary conditions for the momentum equation (6) are $u(y=0) = U$ and $u(y=\delta) = 0$.

The velocity profile for u is found from the solution of Eq. (6), i.e.,

$$u(y) = \frac{1}{2\mu_{\text{f}}}\frac{\partial P}{\partial x}y(y-\delta) + U\left(1 - \frac{y}{\delta}\right) \tag{7}$$

This solution cannot be used yet because it involves the unknown pressure gradient $\partial P/\partial x$. The pressure must be related to the normal force with which the melting block is pushed downward. The pressure distribution is determined first by calculating the liquid flow rate

$$Q_x(x) = \int_0^{\delta} u(x,y)\,\mathrm{d}y \tag{8}$$

By substituting Eq. (7) into Eq. (8), the liquid flow rate is found to be

$$Q_x(x) = -\frac{\delta^3}{12\mu_{\text{f}}}\frac{\mathrm{d}P}{\mathrm{d}x} + \frac{U\delta}{2} \tag{9}$$

2.3. Conservation of mass

As seen from Fig. 3, a mass balance taken over the entire melt layer gives the following relation:

$$VL_xL_z = \widetilde{V}L_xL_z + U\Lambda L_z \tag{10}$$

V is the melting speed of the PCM block, U is the amplitude of the relative motion between the plate and the PCM block, i.e., the velocity of the liquid leaving the melt gap as a consequence of the dragging effect of the plate over a height Λ and $\widetilde{V}$ is the velocity of the liquid leaving the melt gap as a consequence of the squeezing effect maintained by the weight of the PCM. The melting process may be considered quasi-steady if the velocity $\widetilde{V}$ is used in the mass conservation equation instead of the total melting speed V. Rewriting Eq. (10), the relation between the two velocities is

$$\widetilde{V} = V - \frac{U\Lambda}{L_x} \tag{11}$$

Moreover, by invoking the boundary layer theory, the height Λ may be expressed as

$$\frac{\Lambda}{L_x} = f_1(Ste_{\text{eff}}, Re) \approx \frac{f_2(Ste_{\text{eff}})}{Re^n} \tag{12}$$

n and f_2 (Ste_{eff}) are functions to be determined experimentally.

Finally, the mass conservation equation for the melt is

$$\frac{\partial u}{\partial x} + \frac{\partial v}{\partial y} = 0 \tag{13}$$

Integration of this last equation from $y = 0$ $(v = 0)$ to $y = \delta$ $(v = -\widetilde{V})$ yields

$$\frac{\mathrm{d}Q_x(x)}{\mathrm{d}x} = \widetilde{V} \tag{14}$$

Substituting Eq. (9) into (14), the following differential relation between the pressure P, the melting speed V, and the liquid film height δ is obtained

$$\frac{\mathrm{d}^2P}{\mathrm{d}x^2} = -\frac{12\mu_{\text{f}}}{\delta^3}\left[V - U\frac{f_2(Ste_{\text{eff}})}{Re^n}\right] \tag{15}$$

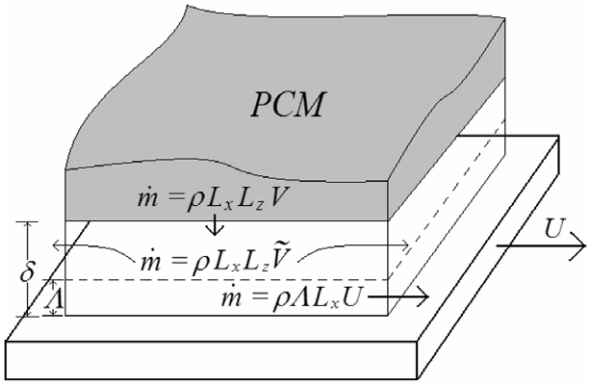

Fig. 3. Mass conservation in the melt layer.

Using the boundary conditions for the pressure P $(x = \pm L_x/2) = 0$, the solution of Eq. (15) is found to be

$$P(x) = \frac{3}{2}\frac{\mu_{\text{f}}}{\delta^3}\left[V - U\frac{f_2(Ste_{\text{eff}})}{Re^n}\right](L_x^2 - 4x^2) \tag{16}$$

Substitution of Eq. (16) into Eq. (5) provides a second relation between the molten layer thickness δ and the melting speed V

$$\frac{\mu_{\text{f}}L_zL_x^3}{\delta^3}\left[V - U\frac{f_2(Ste_{\text{eff}})}{Re^n}\right] = \rho_{\text{s}}L_xL_z(H - S)g \tag{17}$$

2.4. Dimensionless equations

Eqs. (4) and (17) are now cast in dimensionless form using the variables and parameters defined in Table 1

$$-\frac{Ste_{\text{eff}}}{\rho^*} = 1 - \exp(V^*\delta^*Pr_{\text{f}}) \tag{18}$$

$$V^* = \rho^*(H^* - S^*)A{\delta^*}^3 + f_2(Ste_{\text{eff}})Re^{1-n} \tag{19}$$

The above dimensionless equations are easily adapted to the melting of any PCM and for of any geometry. The dimensionless form also facilitates the comparison of the melting behaviour of different PCMs. The Prandtl number Pr_{f} characterizes the substance, the Stefan number Ste_{eff}, the relative heating intensity and the Reynolds number Re, the relative magnitude of the velocity between the plate and the PCM block. Eqs. (18) and (19) represent a system of two equations and two unknowns, V^* and δ^*. Merging both equations yields the following quartic (fourth order) equation for δ^*

$$\rho^*(H^* - S^*)APr_{\text{f}}{\delta^*}^4 + f_2(Ste_{\text{eff}})Pr_{\text{f}}Re^{1-n}\delta^* - \ln(1 + Ste_{\text{eff}}/\rho^*) = 0 \tag{20}$$

The solution is

$$\delta^* = \frac{\sqrt{F(B)}}{2}\left[\frac{128}{27}\frac{(\ln(1 + Ste_{\text{eff}}/\rho^*))^3}{\rho^*(H^* - S^*)APr_{\text{f}}^3(f_2(Ste_{\text{eff}})Re^{1-n})^2}\right]^{1/6} \times \left[\left(\sqrt{\frac{27}{32}}\frac{Pr_{\text{f}}^{3/2}(f_2(Ste_{\text{eff}})Re^{1-n})^2}{(\rho^*(H^* - S^*)A)^{1/2}(F(B)\cdot\ln(1 + Ste_{\text{eff}}/\rho^*))^{3/2}} - 1\right)^{1/2} - 1\right] \tag{21}$$

where $F(B) = \left(\frac{-1}{[1+\sqrt{1+B}]^{1/3}} + \frac{-1}{[1-\sqrt{1+B}]^{1/3}}\right)$ and $B = \frac{256}{27}\frac{\rho^*(H^* - S^*)A(\ln(1+Ste_{\text{eff}}/\rho^*))^3}{Pr_{\text{f}}^3(f_s(Ste_{\text{eff}})Re^{1-n})^4}$.

Table 1
Dimensionless variables and parameters

δ^*	δ/L_x
H^*	H/L_x
S^*	S/L_x
V^*	VL_x/ν_{f}
ρ^*	ρ_s/ρ_{f}
t^*	$\nu_{\text{f}}t/L_x^2$
A	L_x^3g/ν_{f}^2

The melting speed V^* is then obtained by substituting the solution (21) back into Eq. (18) or (19). Finally, recalling that $dS^*/dt^* = V^*$ and $S^*(t^* = 0) = 0$, the time varying height of the block is obtained numerically using a fourth order Runge–Kutta integration scheme.

2.5. Effective Stefan number

The effective Stefan number Ste_{eff} introduced in Eq. (12) takes into account the subcooling of the PCM. The net effect of subcooling is to slow down the melting process as some of the heat released by the heated plate is stored as sensible heat in the solid phase of the PCM block. The effective Stefan number is defined as

$$Ste_{\text{eff}} = \frac{C_f \Delta T}{(h_{fs} + C_s T_{sc})} \tag{22}$$

which can be rewritten as

$$Ste_{\text{eff}} = \frac{Ste}{(1 + Ste_{sc})} \tag{23}$$

3. Experimental setup

In order to study close contact melting of ice with a moving heated flat plate and to assess the validity of the above analytical model, an experimental apparatus was designed and built (Fig. 4). The effect of an infinite moving flat plate is mimicked with a rotating highly polished aluminium disk, 56 cm in diameter, 2.5 cm in thickness and weighting 11.5 kg (Fig. 5(a)). The disk is attached to a vertical shaft rotated by a DC, variable speed, 1/8 hp electric motor. The speed of rotation varies from 0 to 1000 rpm (0–24 m/s, linear velocity). The aluminium disk is heated by four electrical resistances (Fig. 5(b)) that provide a maximum of 6.5 kW at 240 V. The temperature of the disk is maintained with a temperature controller (series CN77000) from micromega and with an on/off solid state relay (series SSRL240) from Omega. An infrared thermocouple OS37-10 (J-type, accurate to ± 2 K), also from Omega, is used to measure the surface temperature of the rotating disk.

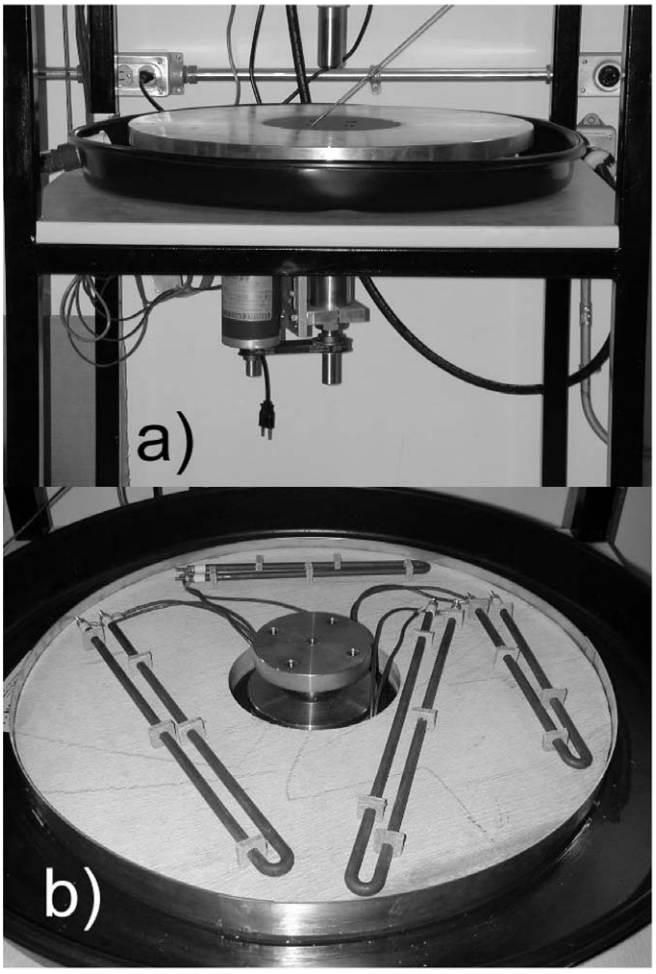

Fig. 5. Experimental setup: (a) aluminium disk and DC electric motor and (b) heating resistances.

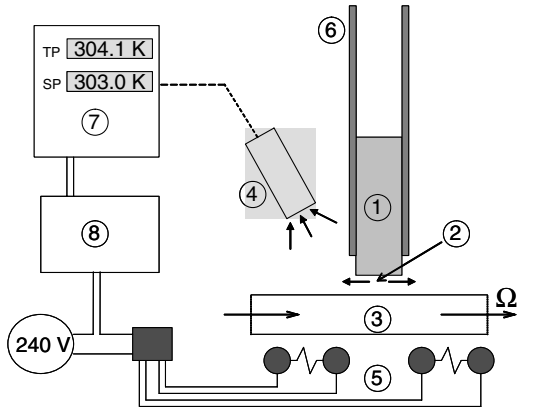

Fig. 4. Schematic of the experimental setup.

During an experiment, a block of sub cooled ice ($T_{sc} = 22$ K), prepared with tap water, 0.03 m wide, 0.03 m deep and 0.076 m high, held in a rectangular duct made with plexiglass walls, presses against the surface of the disk under its own weight. A plastic wiper is also used to remove any excess liquid that could remain on the disk. The time varying height of the melting ice block is measured with a ruler, fixed to the transparent wall of the duct, and with a stop watch.

4. Results and discussion

A series of experiments were conducted for two disk temperatures of 299 K and 318 K (which correspond to Stefan numbers Ste_{eff} of 0.380 and 0.640 respectively) and

for different speeds of rotation raging from 80 rpm to 1000 rpm (which correspond to Reynolds numbers ranging from 5.8×10^4 to 9.3×10^5).

First, the effect of the curvature of the heated surface (rotating disk) on the melting process was examined (the linear speed seen by the PCM block resting on a circular surface is not constant along its length L_z). The results are reported in Fig. 6(a) and (b) for two melting scenarios. The error bars represent the area of multiple data measured under identical conditions. By taking into account the experimental uncertainties, it is seen that the measured melting profiles ($(H^* - S^*)$ versus t^*) recorded at two different positions on the rotating disk (radius $R = 0.119$ m and $R = 0.241$ m.) are nearly the same. In both cases, the linear speeds are identical, i.e., the Reynolds numbers are similar. Nevertheless, to minimize the effect of curvature of the heated surface, that is to mimic the motion of an infinite heated flat plate, all experiments reported here were performed at a radius $R = 0.241$ m.

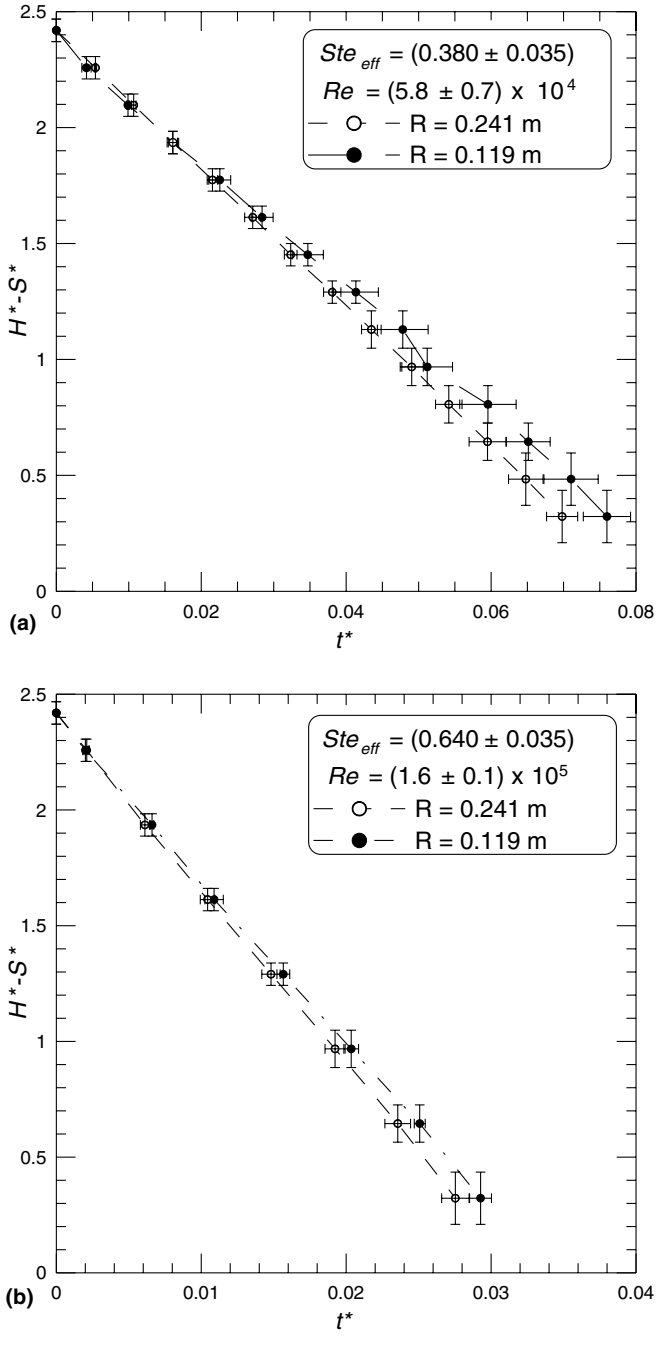

Fig. 6. $H^* - S^*$ versus t^*: effect of curvature for two different radii: (a) $Ste_{\text{eff}} = 0.380$ and $Re = 5.8 \times 10^4$ and (b) $Ste_{\text{eff}} = 0.640$ and $Re = 1.6 \times 10^5$.

Fig. 7 shows the measured time periods needed to melt 87% of the ice block as a function of the Reynolds number for the two different plate temperatures. Due to the physical limitations of the experimental setup, it was impossible to properly measure the complete melting time. As a result, the last measured melting time was obtained when 87% of the ice block had melted. Examination of this figure reveals three distinct melting regimes. For $Re < 3 \times 10^5$, referred to as the contact melting regime, the relative motion between the heated plate and the ice block is small enough so that heat transfer is dominated by close contact melting. The melting rate increases with Re and Ste_{eff} (Fig. 8(a) and (b)) while the melting speed V remains nearly constant throughout the melting process. It is independent of the time varying weight of the ice block. It also implies that the melt layer thickness δ^* is independent of the time varying weight of the ice block.

In the abrasion regime, i.e. for $Re > 5 \times 10^5$, the relative velocity is large enough so that no melt layer is observed between the heated surface and the ice block. From time to time, small pieces of ice detach from the PCM block indicating that the melting process is dominated by abrasion. Heat transfer is therefore due to conduction across the actual contact spots between two moving rough surfaces and radiation across the gaps. Compared to the

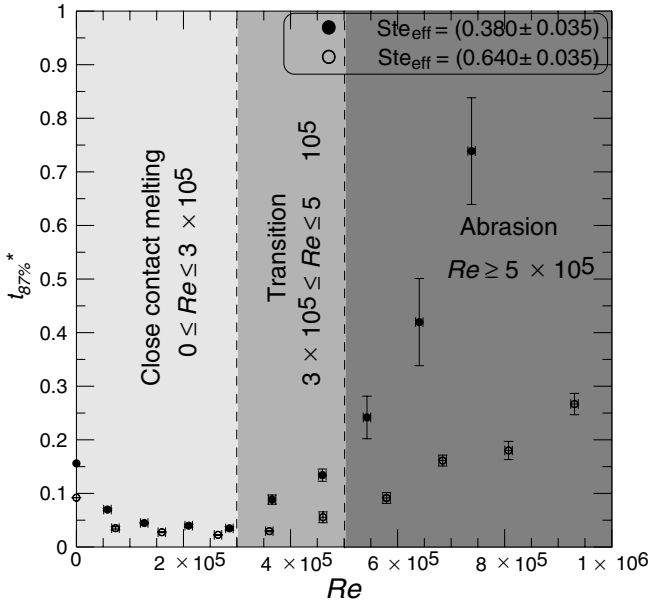

Fig. 7. Experimental results for $t^*_{87\%}$ versus Re.

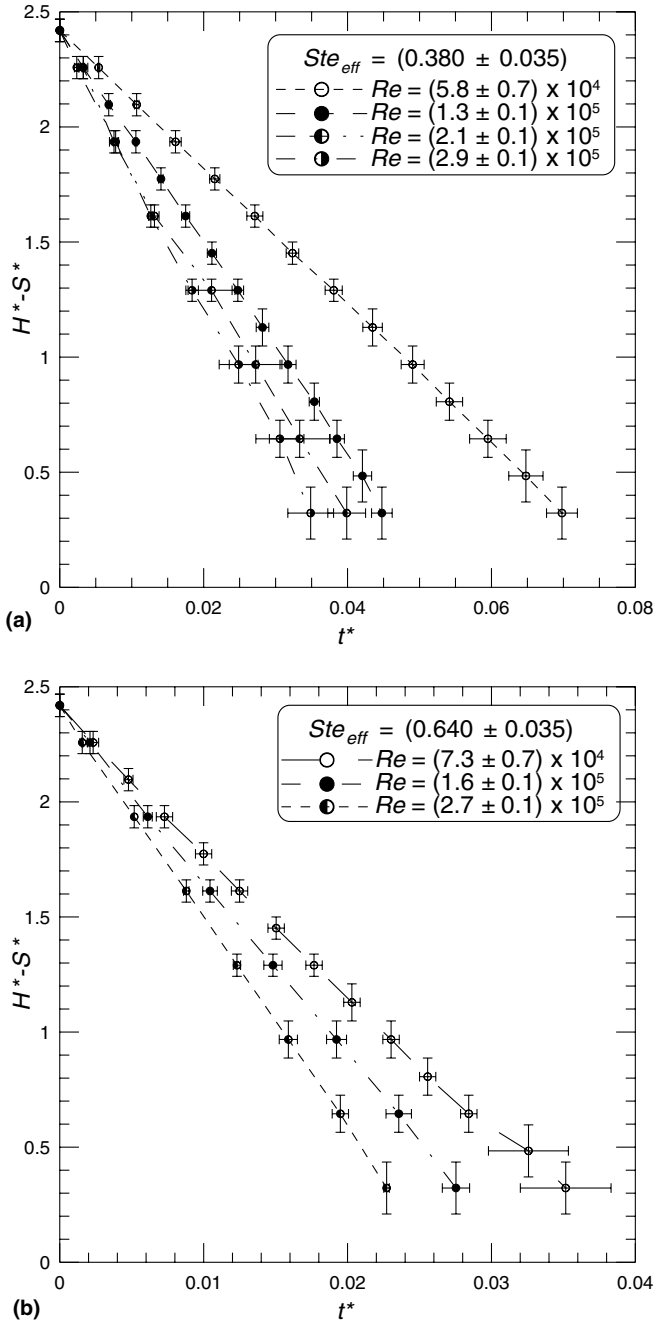

Fig. 8. $H^* - S^*$ versus t^* in the close contact melting regime for (a) $Ste_{\text{eff}} = 0.380$ and (b) $Ste_{\text{eff}} = 0.640$.

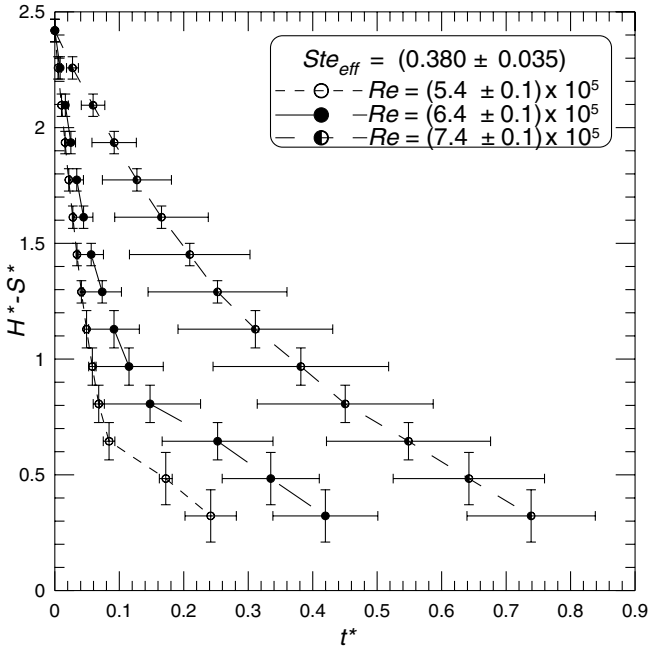

Fig. 9. $H^* - S^*$ versus t^* for $Ste_{\text{eff}} = 0.380$ in the abrasion regime.

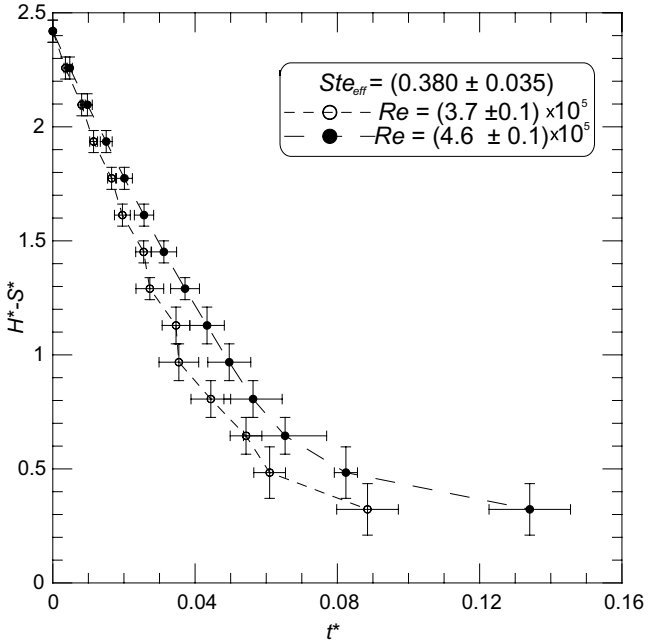

Fig. 10. $H^* - S^*$ versus t^* for $Ste_{\text{eff}} = 0.380$ in the transition regime.

contact melting regime for which the gaps are filled with melt, the thermal contact resistance is much larger in the abrasion regime and, as a result, the melting speed slows down considerably (Fig. 9).

Finally, for $3 \times 10^5 < Re < 5 \times 10^5$, a transition zone bridges the contact melting regime to the abrasion regime. The dimensionless melting profiles ($(H^* - S^*)$ versus t^*) for this case are reported in Fig. 10.

Fig. 11(a) and (b) compare the measured and the predicted melting profiles in the close contact melting regime for $Ste_{\text{eff}} = 0.38$ and $Ste_{\text{eff}} = 0.64$ respectively. The functions in Eq. (12), i.e., $n = 0.57$ and $f_2(Ste_{\text{eff}}) = 0.7 \cdot Ste_{\text{eff}}$, were determined from the above experimental results using a trial and error method aimed at finding the functional forms for n and f_2 that provided the best agreement between the experimental data and the mathematical model. In spite of the measurement uncertainties and the simplicity of the model, the agreement between the experimental data and the predictions is excellent.

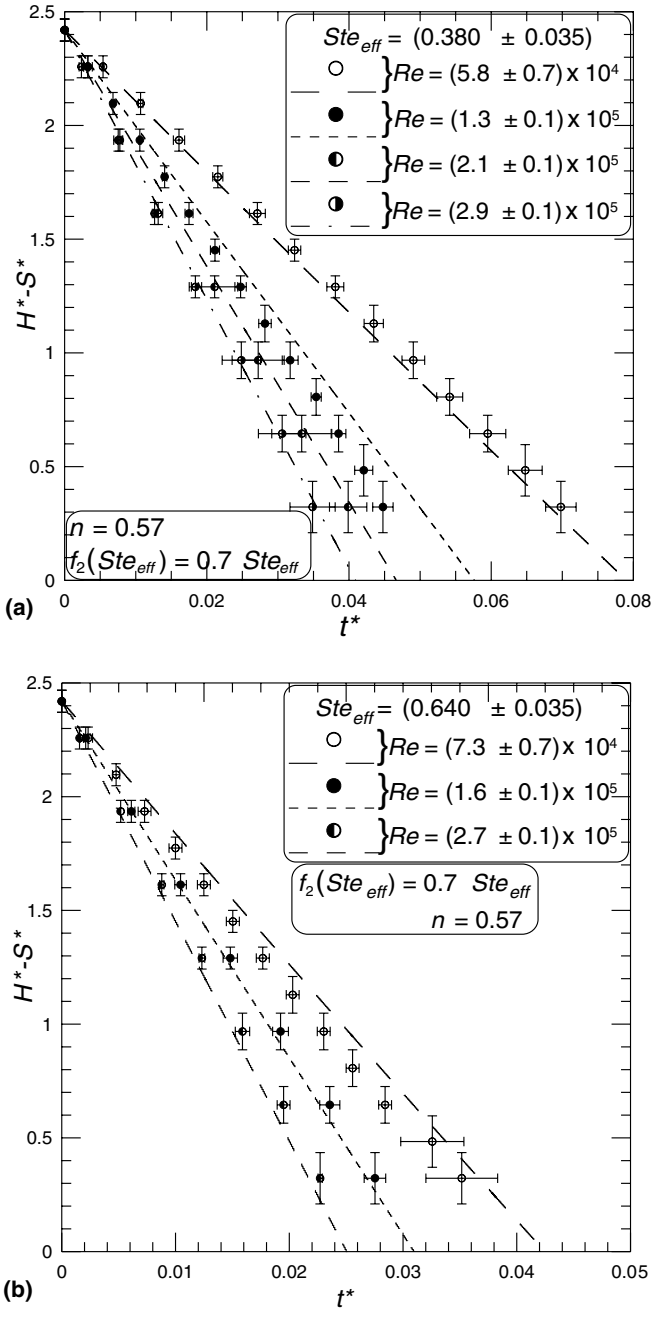

Fig. 11. $H^* - S^*$ versus t^*, experiments versus predictions for (a) $Ste_{\text{eff}} = 0.380$ and (b) $Ste_{\text{eff}} = 0.640$.

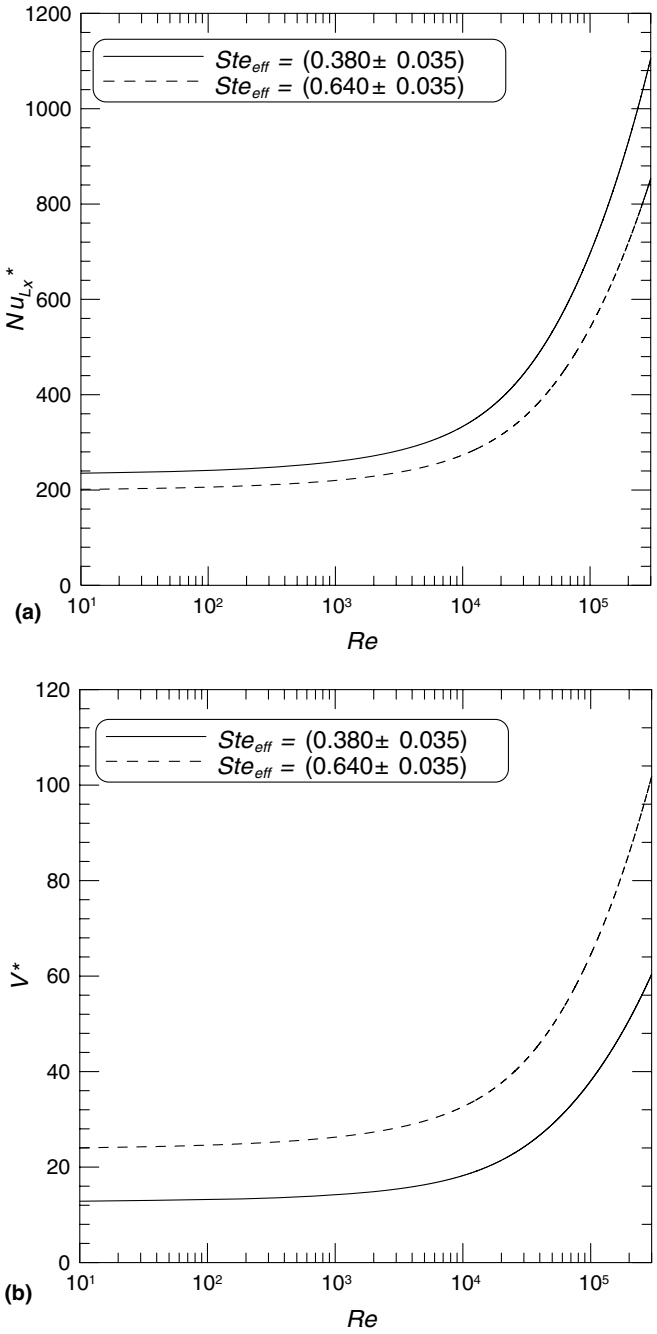

Fig. 12. (a) Nu_{L_x} versus Re for $Ste_{\text{eff}} = 0.380$ and 0.640, (b) V^* versus Re for $Ste_{\text{eff}} = 0.380$ and 0.640.

The predicted variation of the Nusselt number Nu_{L_x} and melting speed V^* as a function of the Reynolds number Re at the melting interface are depicted in Fig. 12(a) and (b) respectively. The Nusselt number is defined here as

$$Nu_{L_x} = \frac{q''}{(k_f \Delta T / L_x)} = -\frac{(\mathrm{d}T/\mathrm{d}y|_{y=\delta})}{(\Delta T / L_x)} \tag{24}$$

The melting speed is related to the Nusselt number via the following expression:

$$V^* = \frac{Ste_{\text{eff}}}{\rho^* Pr_f} Nu_{L_x} \tag{25}$$

It is seen that the Nusselt number and the melting speed increase with the Reynolds number. This behaviour is due to the fact that the thickness of the melt layer δ^* diminishes as Re augments (the drag on the moving surface augments) (Fig. 13). The relative velocity between the PCM block and the plate starts to play an important role in the melting process when $Re > 10^4$. Finally, based on the experimental results and on the analytical predictions, the close contact melting regime may also be characterized by a melt layer thickness $\delta^* > 8 \times 10^{-4}$ while the abrasion regime prevails for $\delta^* < 8 \times 10^{-4}$. These thicknesses are only valid for the

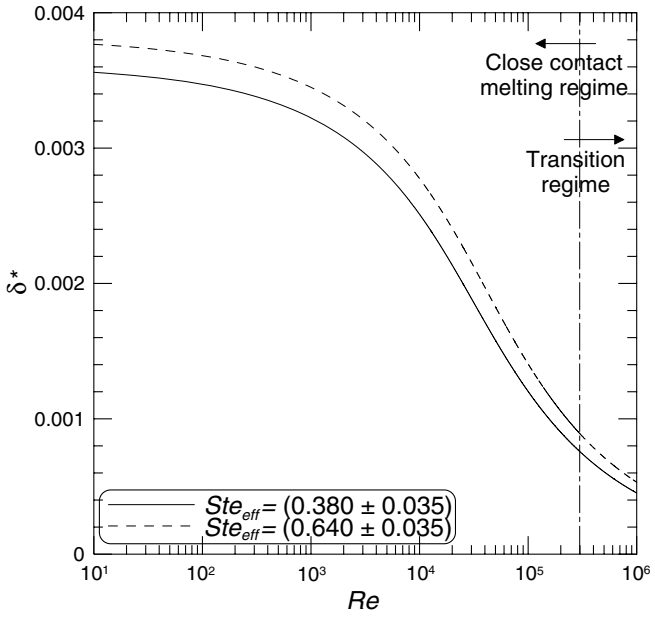

Fig. 13. δ^* versus Re for $Ste_{\text{eff}} = 0.380$ and 0.640.

case of a PCM melting on a smooth highly polished heated flat plate. Further investigations are needed in order to characterize the effects of the surface roughness on the melting process.

5. Concluding remarks

A study was conducted to examine the effect of the relative motion between a high Prandtl number PCM block and a heated flat plate in the process of close contact melting. An analytical model, resting on the boundary layer theory, was proposed and its predictions were compared and validated with experimental data. The main conclusions of this study are as follows:

- The effect of the relative motion between the PCM block and the heated plate on close contact melting becomes perceptible for $Re > 10^4$.
- Three different melting regimes from a moving heated plate are identified: for $Re < 3 \times 10^5$, close contact melting is the dominant mode of heat transfer in the melt layer; for $Re > 5 \times 10^5$, the thickness of the liquid melt layer becomes so small that the melting process is hindered. Abrasion prevails. For $3 \times 10^5 < Re < 5 \times 10^5$, a transition zone bridges the contact melting regime to the abrasion regime.
- In the close contact melting regime, the melting time may be reduced by up to 66% compare to the melting time from an immobile heated plate.
- Close contact melting is the dominant mode of heat transfer for melt layer thickness $\delta^* > 8 \times 10^{-4}$ while the abrasion regime prevails for $\delta^* < 8 \times 10^{-4}$.

Acknowledgements

The authors are grateful to the Natural Sciences and Engineering Research council of Canada and to the Fonds Québécois de la Recherche sur la nature et les technologies for their financial support.

References

[1] A. Bejan, Contact melting heat transfer and lubrication, Adv. Heat Transfer 24 (1994) 1–38.
[2] A.J. Fowler, A. Bejan, Contact melting during sliding on ice, Int. J. Heat Mass Transfer 36 (5) (1993) 1171–1179.
[3] W.G. Park, M.S. Park, Y.R. Jung, K.L. Jang, Numerical study of defrosting phenomena of automotive windshield glass, Numer. Heat Transfer, Part A: Appl. 47 (2005) 725–739.
[4] K.A.R. Ismail, A.B. de Jesus, Modeling and solution of the solidification problem of PCM around a cold cylinder, Numer. Heat Transfer, Part A: Appl. 36 (1999) 95–114.
[5] J.M. Khodadadi, Y. Zhang, Effects of buoyancy-driven convection on melting within spherical containers, Int. J. Heat Mass Transfer 44 (2001) 1605–1618.
[6] M.K. Moallemi, B.W. Webb, R. Viskanta, An experimental and analytical study of close-contact melting, J. Heat Transfer 108 (1986) 894–899.
[7] I. Sezai, A.A. Mohamad, Natural convection in a rectangular cavity heated from below and cooled from the top as well as the sides, Phys. Fluids 12 (2) (2000) 432–443.
[8] M. Ibrahim, P. Sokolov, T. Kerslake, C. Tolbert, Experimental and computational investigations of phase change thermal energy storage canisters, J. Sol. Energy Eng. 122 (2000) 176–182.
[9] J. Blackwood, F. Wessling, Design of thermal initial and boundary conditions to control the expansion of water-based phase-change materials in low gravity, Numer. Heat Transfer, Part A: Appl. 49 (2006) 525–542.
[10] D. Veilleux, E. Gonçalves, M. Faghri, Y. Asako, M. Charmchi, Phase change in a three-dimensional rectangular cavity under electromagnetically simulated low gravity: top wall heating with an unfixed material, Numer. Heat Transfer, Part A: Appl. 48 (2005) 849–878.
[11] Y. Asako, M. Faghri, Effect of density change on melting of unfixed rectangular phase-change material under low-gravity environment, Numer. Heat Transfer, Part A: Appl. 36 (1999) 825–838.
[12] Y. Asako, E. Gonçalves, M. Faghri, M. Charmchi, Numerical solution of melting processes for fixed and unfixed phase change material in the presence of magnetic field—simulation of low-gravity environment, Numer. Heat Transfer, Part A: Appl. 42 (2002) 565–583.
[13] H. Hong, A. Saito, Numerical method for direct contact melting in transient process, Int. J. Heat Mass Transfer 36 (1993) 2093–2103.
[14] A. Saito, H. Hong, O. Hirokane, Heat transfer enhancement in the direct contact melting process, Int. J. Heat Mass Transfer 35 (1992) 295–305.
[15] M. Lacroix, Contact melting of a phase change material inside a heated parallelepipedic capsule, Energy Convers. Manage. 42 (2001) 35–47.
[16] M. Bareiss, H. Beer, An analytical solution of the heat transfer process during melting of an unfixed solid phase change material inside a horizontal tube, Int. J. Heat Mass Transfer 27 (1984) 739–745.
[17] A. Saito, Y. Utaka, M. Akiyoshi, K. Katayama, On the contact heat transfer with melting (2nd report: analytical study), Bull. JSME 28 (1985) 1703–1709.
[18] H. Kumano, A. Saito, S. Okawa, Y. Yamada, Direct contact melting with asymmetric load, Int. J. Heat Mass Transfer 48 (2005) 3221–3230.

[19] H. Kumano, A. Saito, S. Okawa, K. Takeda, A. Okuda, Study of direct contact melting with hydrocarbon mixtures as the PCM, Int. J. Heat Mass Transfer 48 (2005) 3212–3220.
[20] S.K. Roy, S. Sengupta, The melting process within spherical enclosures, J. Heat Transfer 109 (1987) 460–462.
[21] T. Hirata, Y. Makino, Y. Kaneko, Analysis of close-contact melting for octadecane and ice inside isothermally heated horizontal rectangular capsule, Int. J. Heat Mass Transfer 34 (1991) 3091–3106.
[22] W.Z. Chen, S.M. Cheng, Z. Luo, W.M. Gu, Analysis of contact melting of phase change materials inside a heated rectangular capsule, Int. J. Energy Res. 19 (1995) 337–345.
[23] A. Bejan, Convection Heat Transfer, second ed., Wiley Interscience Publication, New York, 1995, pp. 434–438.
[24] D. Groulx, M. Lacroix, Effects of convection and inertia on close contact melting, Int. J. Therm. Sci. 42 (2003) 1073–1080.
[25] K. Taghavi, Analysis of direct-contact melting under rotation, J. Heat Transfer 112 (1990) 137–143.
[26] H. Yoo, Analytical solutions to unsteady close-contact melting on a flat plate, Int. J. Heat Mass Transfer 43 (2000) 1457–1467.
[27] H. Yoo, Initial transient behaviour during close-contact melting induced by convective heating, Int. J. Heat Mass Transfer 44 (2001) 2193–2197.
[28] D.A. Knoll, D.B. Kothe, B. Lally, A new nonlinear solution method for phase-change problems, Numer. Heat Transfer, Part B: Fund. 35 (1999) 439–459.
[29] C.K. Chun, S. O Park, A fixed-grid finite-difference method for phase-change problems, Numer. Heat Transfer, Part B: Fund. 38 (2000) 59–73.
[30] C. Ho, J. Lin, S. Chiu, Heat transfer of solid–liquid phase-change material suspensions in circular pipes: effects of wall conduction, Numer. Heat Transfer, Part A: Appl. 45 (2004) 171–190.